World Academy of Science, Engineering and Technology
International Journal of Mechanical and Mechatronics Engineering
Vol:8, No:10, 2014

Analysis of a Self-Acting Air Journal Bearing: Effect of Dynamic Deformation of Bump Foil

H. Bensouilah, H. Boucherit, M. Lahmar

***Abstract*—**A theoretical investigation on the effects of both steady-state and dynamic deformations of the foils on the dynamic performance characteristics of a self-acting air foil journal bearing operating under small harmonic vibrations is proposed. To take into account the dynamic deformations of foils, the perturbation method is used for determining the gas-film stiffness and damping coefficients for given values of excitation frequency, compressibility number, and compliance factor of the bump foil. The nonlinear stationary Reynolds' equation is solved by means of the Galerkins' finite element formulation while the finite differences method are used to solve the first order complex dynamic equations resulting from the perturbation of the nonlinear transient compressible Reynolds' equation. The stiffness of a bump is uniformly distributed throughout the bearing surface (generation I bearing). It was found that the dynamic properties of the compliant finite length journal bearing are significantly affected by the compliance of foils especially whenthe dynamic deformation of foils is considered in addition to the static one by applying the principle of superposition.

***Keywords*—**Elasto-aerodynamic lubrication, Air foil bearing, Steady-state deformation, Dynamic deformation, Stiffness and damping coefficients, Perturbation method, Fluid-structure interaction, Galerk infinite element method, Finite difference method.

I. Introduction

AIR foil bearings so-called aerodynamic journal bearings are the machine components which find nowadays widespread use in very high speed, lightly loaded oil-free rotating turbo machinery because they have theoretically no speed limitations, and they are environmentally benign. In the design of such bearings, it is of cardinal importance to enhance their steady state and dynamic performance characteristics for the safety operation, especially against the external dynamic excitations [1], [2]. Fig. 1 shows a schematic picture of a typical elastically supported foil bearing. As illustrated, it schematically consists of a cylindrical shell (sleeve) lined with corrugated bumps (bump foil) topped with a thin flat foil (top foil). The bump foil serves as a support for the top metal foil and its compliant feature allows the top foil to deform under the action of aerodynamic pressure. This latter is generated in the air film when the shaft (journal) rotates over a certain angular speed. Air foil bearings were constantly modified several times in order to improve their performances. In fact, there are three generations of air foil bearings. One distinguishes one generation from another by the complexity of the spring resistance in the bump foil. The latest bump foil bearings being developed are of the so-called "generation III" variety [3], [4]. The bumps of the first designs of these bearings, so-called generation I, are uniformly stiff. Generation II bump foils vary but only on one axis. In generation III bearings, however, the stiffness of the bumps is varied to optimize air film pressure. This complex variation of bump stiffness increases the load capacity of generation III bearings to more than twice that of best previous generation designs. Historically, air foil bearings first came into wide-spread use in the 1960's, when they began to appear in such applications as the air-cycle machines (ACM) that cool and pressurize commercial and military airplanes and, more recently, natural-gas compressors. These bearings have several advantages over oil lubricated bearings [5].

H. Bensouilah is with the Mechanical Engineering Department, Guelma University, BP 401, Guelma 24000, Algeria (phone: 00213-37261889; e-mail: hamzabensouilah52@gmail.com).
H. Boucherit and M. Lahmar are with the Mechanical Engineering Department, Guelma University, BP 401, Guelma 24000, Algeria.

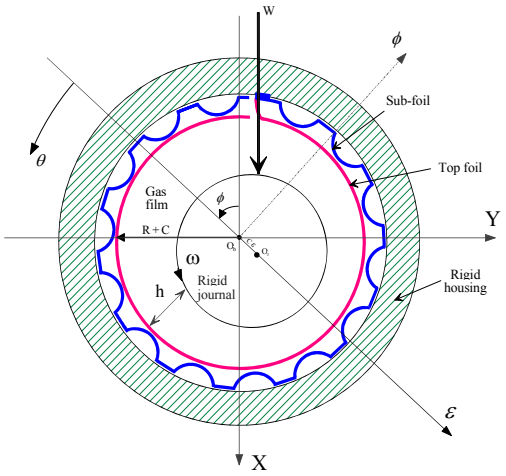

Fig. 1 Cross section schematic of a typical foil bearing

They have theoretically no speed limitations, and they usually work better at temperature extremes than oil bearings because most oils break down at very high temperatures and become overly viscous at low temperatures [4]. Besides, they require less maintenance and they can be stored indefinitely, unlike oiled bearings, which must be cleaned and run periodically. And they are environmentally benign. On the other hand, an engine that incorporates air foil bearings will be lighter than its oil-dependent counterpart [6]. Foil bearings are somewhat lighter than the ball bearings they replace. This is due to the elimination of the lubrication system (pumps, filters, plumbing and so on) that oil-lubricated bearings require [7], [8]. Over the past decades, a considerable number of theoretical and experimental studies have been made on the performance characteristics of air-lubricated bearings by many

researchers [9]. As far as we know, there are very few research works treating the dynamic properties of such bearings by taking into consideration the dynamic deformation of foils in addition to the static one even for highly loaded bearings. The main objective of the present research is to theoretically investigate the stiffness and damping characteristics of a compliant self-acting air lubricated bearing by considering both static and dynamic deformations of the bearing structure which is built up with thin metal foils by applying the principle of superposition. In addition, one desires to determine how these rotor-dynamic coefficients vary with some operating conditions, such as dynamic excitation frequency. The rotor-dynamic coefficients will be determined from the view point of linear dynamics, i.e. for small harmonic vibrations amplitudes of the rigid rotor using a perturbation method, and will serve as input data for the stability and unbalance response analyses of rotor-bearing system. The calculations are generally performed for the following cases: (1) rigid gas bearing, (2) only static deformation of the bearing structure is considered, (3) both static and dynamic deformations are taken into account.

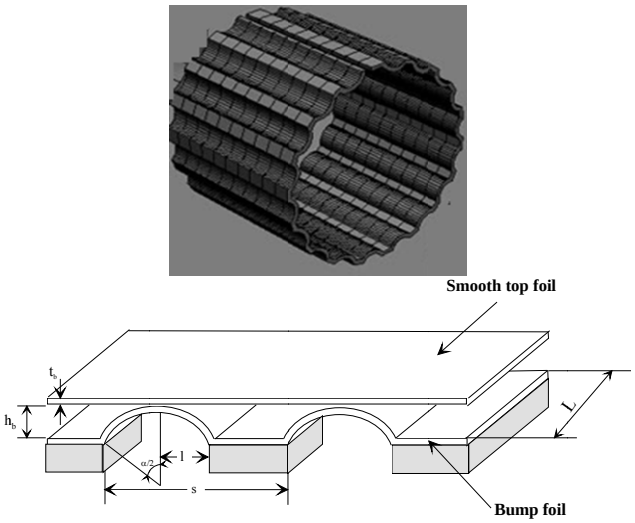

Fig. 2 Detailed configuration of the bump foil

II. Mathematical Formulation

A. Steady-State Film Thickness Expression

For a compliant journal bearing, the steady-state film thickness is calculated by

$$h_0 = C\left(1+\varepsilon_0\cos\theta\right)+U_0 \tag{1}$$

where U_0 is the radial deformation of the bump foil due to the steady-state aerodynamic pressure. As a first approximation, the corrugated sub-foil is modeled as a simple Winkler elastic foundation, i.e. the stiffness of a bump is uniformly distributed throughout the bearing surface (isotropic stiffness). With this consideration, the steady-state radial deformation of a bump is proportional to the pressure difference $(p_0 - p_a)$, i.e.

$$U_0 = L_0\left(p_0 - p_a\right) \tag{2}$$

where p_0 and p_a are the steady-state gas-film and ambient pressures, respectively.

$$L_0 = \frac{2s}{E}\left(\frac{l}{t_b}\right)^3\left(1-\sigma^2\right)$$

represents the compliance of the bump foil, inversely proportional to the bump foil stiffness K_b. As depicted in Fig. 2,s is the bump pitch, l is half of the bump length, t_b is the bump foil thickness, E and σ are the Young's modulus and Poisson's ratio of bump foil material, respectively [1]. Accordingly, the steady-state film thickness is written as

$$h_0 = C\left(1+\varepsilon_0\cos\theta\right)+L_0\left(p_0 - p_a\right) \tag{3}$$

In dimensionless form, (3) reads

$$\tilde{h}_0 = 1+\varepsilon_0\cos\theta+\alpha\left(\tilde{p}_0-1\right) \tag{4}$$

where α is the dimensionless compliance operator defined as:

$$\alpha = \frac{2p_a s}{CE}\left(\frac{l}{t_b}\right)^3\left(1-\sigma^2\right)$$

B. Steady-State and Dynamic Compressible Reynolds' Equations, and Boundary Conditions

If we assume that the journal (rotor) is excited into a simple harmonic motion of small amplitudes within the compliant bearing at frequency ν, the instantaneous eccentricity ratio and attitude angle may be expressed respectively as [10]:

$$\varepsilon = \varepsilon_0 + \Delta\varepsilon\, e^{i\gamma\tilde{\tau}} \text{ and } \phi = \phi_0 + \Delta\phi\, e^{i\gamma\tilde{\tau}};$$
$$\left|\Delta\varepsilon\right| << \varepsilon_0\,, \left|\Delta\phi\right| << \phi_0 \text{ and } i=\sqrt{-1} \tag{5}$$

where $\gamma = \nu/\omega$ is the relative excitation frequency, and $\Delta\varepsilon$ and $\Delta\phi$ are complex amplitudes of eccentricity ratio and attitude angle, respectively. Under these conditions, the transient hydrodynamic lubrication problem is governed by the following differential equations whose the unknown functions are the steady state air-film pressure $\tilde{p}_0$, and the complex dynamic pressures $\tilde{Q}_\varepsilon$ and $\tilde{Q}_\phi$:

$$\frac{\partial}{\partial\theta}\left(\tilde{p}_0\tilde{h}_0^3\frac{\partial\tilde{p}_0}{\partial\theta}\right)+\lambda\frac{\partial}{\partial\tilde{z}}\left(\tilde{p}_0\tilde{h}_0^3\frac{\partial\tilde{p}_0}{\partial\tilde{z}}\right)=\Lambda\frac{\partial}{\partial\theta}\left(\tilde{p}_0\tilde{h}_0\right) \tag{6}$$

$$\frac{\partial}{\partial\theta}\left[\tilde{h}_0^{\,3}\tilde{p}_0\frac{\partial\tilde{Q}_\varepsilon}{\partial\theta}\right]+\lambda\frac{\partial}{\partial\tilde{z}}\left[\tilde{h}_0^{\,3}\tilde{p}_0\frac{\partial\tilde{Q}_\varepsilon}{\partial\tilde{z}}\right]+$$
$$\tilde{h}_0^{\,3}\tilde{p}_0\left[\frac{\partial\tilde{p}_0}{\partial\theta}\frac{\partial}{\partial\theta}\left(\frac{\tilde{Q}_\varepsilon}{\tilde{p}_0}\right)+\lambda\frac{\partial\tilde{p}_0}{\partial\tilde{z}}\frac{\partial}{\partial\tilde{z}}\left(\frac{\tilde{Q}_\varepsilon}{\tilde{p}_0}\right)\right]+ \quad (7)$$
$$\Lambda\frac{\partial}{\partial\theta}\left(\tilde{p}_0\tilde{h}_0\right)\left[\frac{\tilde{Q}_\varepsilon}{\tilde{p}_0}+3\frac{\tilde{h}_\varepsilon}{\tilde{h}_0}\right]+$$
$$3\tilde{h}_0^{\,3}\tilde{p}_0\left[\frac{\partial\tilde{p}_0}{\partial\theta}\frac{\partial}{\partial\theta}\left(\frac{\tilde{h}_\varepsilon}{\tilde{h}_0}\right)+\lambda\frac{\partial\tilde{p}_0}{\partial\tilde{z}}\frac{\partial}{\partial\tilde{z}}\left(\frac{\tilde{h}_\varepsilon}{\tilde{h}_0}\right)\right]=$$
$$\Lambda\frac{\partial}{\partial\theta}\left[\tilde{p}_0\tilde{h}_0\left(\frac{\tilde{h}_\varepsilon}{\tilde{h}_0}+\frac{\tilde{Q}_\varepsilon}{\tilde{p}_0}\right)\right]+2\Lambda i\gamma\tilde{p}_0\tilde{h}_0\left(\frac{\tilde{h}_\varepsilon}{\tilde{h}_0}+\frac{\tilde{Q}_\varepsilon}{\tilde{p}_0}\right)$$

with $\tilde{h}_\varepsilon=\cos\theta+\tilde{U}_\varepsilon$

$$\frac{\partial}{\partial\theta}\left[\tilde{h}_0^{\,3}\tilde{p}_0\frac{\partial\tilde{Q}_\phi}{\partial\theta}\right]+\lambda\frac{\partial}{\partial\tilde{z}}\left[\tilde{h}_0^{\,3}\tilde{p}_0\frac{\partial\tilde{Q}_\phi}{\partial\tilde{z}}\right]+$$
$$\tilde{h}_0^{\,3}\tilde{p}_0\left[\frac{\partial\tilde{p}_0}{\partial\theta}\frac{\partial}{\partial\theta}\left(\frac{\tilde{Q}_\phi}{\tilde{p}_0}\right)+\lambda\frac{\partial\tilde{p}_0}{\partial\tilde{z}}\frac{\partial}{\partial\tilde{z}}\left(\frac{\tilde{Q}_\phi}{\tilde{p}_0}\right)\right]+ \quad (8)$$
$$\Lambda\frac{\partial}{\partial\theta}\left(\tilde{p}_0\tilde{h}_0\right)\left[\frac{\tilde{Q}_\phi}{\tilde{p}_0}+3\frac{\tilde{h}_\phi}{\tilde{h}_0}\right]+$$
$$3\tilde{h}_0^{\,3}\tilde{p}_0\left[\frac{\partial\tilde{p}_0}{\partial\theta}\frac{\partial}{\partial\theta}\left(\frac{\tilde{h}_\phi}{\tilde{h}_0}\right)+\lambda\frac{\partial\tilde{p}_0}{\partial\tilde{z}}\frac{\partial}{\partial\tilde{z}}\left(\frac{\tilde{h}_\phi}{\tilde{h}_0}\right)\right]=$$
$$\Lambda\frac{\partial}{\partial\theta}\left[\tilde{p}_0\tilde{h}_0\left(\frac{\tilde{h}_\phi}{\tilde{h}_0}+\frac{\tilde{Q}_\phi}{\tilde{p}_0}\right)\right]+2\Lambda i\gamma\tilde{p}_0\tilde{h}_0\left(\frac{\tilde{h}_\phi}{\tilde{h}_0}+\frac{\tilde{Q}_\phi}{\tilde{p}_0}\right)$$

with $\tilde{h}_\phi=\sin\theta+\tilde{U}_\phi$

It is noted that (6) is a nonlinear equation while (7) and (8) are complex linear with equations respect to $\tilde{Q}_\varepsilon$ and $\tilde{Q}_\phi$, and they are easily solved if the steady-state film thickness $\tilde{h}_0$ and steady-state pressure field $\tilde{p}_0$ are obtained from (4) and (6).

The boundary conditions associated to these equations are:

$$\tilde{p}_0=1\,\text{at}\,\tilde{z}=\pm\tfrac{1}{2} \quad (9a)$$

$$\tilde{p}_0(\theta=0,\tilde{z})=\tilde{p}_0(\theta=2\pi,\tilde{z})=1 \quad (9b)$$

$$\tilde{p}_0(\theta=\theta_2,\tilde{z})=1,\ \text{and}\ \frac{\partial\tilde{p}_0}{\partial\theta}(\theta=\theta_2,\tilde{z})=0 \quad (9c)$$

and

$$\tilde{Q}_\varepsilon=\tilde{Q}_\phi=0\,\text{at}\,\tilde{z}=\pm\tfrac{1}{2} \quad (10a)$$

$$\tilde{Q}_\varepsilon(\theta=0,\tilde{z})=\tilde{Q}_\varepsilon(\theta=2\pi,\tilde{z})=0 \quad (10b)$$

$$\tilde{Q}_\phi(\theta=0,\tilde{z})=\tilde{Q}_\phi(\theta=2\pi,\tilde{z})=0 \quad (10c)$$

C. Fluid-Film Dynamic Coefficients

The complex distributions $\tilde{Q}_\varepsilon$ and $\tilde{Q}_\phi$ are obtained from (7) and (8) from which the eight dynamic coefficients in the ε, ϕ-coordinate system can be calculated by integrations:

$$Z_{\varepsilon\varepsilon}=-2\int_0^{2\pi}\int_0^{1/2}\tilde{Q}_\varepsilon\cos\theta\,d\tilde{z}d\theta;\ Z_{\varepsilon\varphi}=-2\int_0^{2\pi}\int_0^{1/2}\tilde{Q}_\varphi\cos\theta\,d\tilde{z}d\theta$$
$$Z_{\varphi\varepsilon}=-2\int_0^{2\pi}\int_0^{1/2}\tilde{Q}_\varepsilon\sin\theta\,d\tilde{z}d\theta;\ Z_{\varphi\varphi}=-2\int_0^{2\pi}\int_0^{1/2}\tilde{Q}_\varphi\sin\theta\,d\tilde{z}d\theta \quad (11)$$

where $Z_{\varepsilon\varepsilon}=A_{\varepsilon\varepsilon}+i\gamma B_{\varepsilon\varepsilon}$, etc. are the dimensionless complex impedances, and $A_{\varepsilon\varepsilon}=\text{Re}\,al(Z_{\varepsilon\varepsilon})$, and $B_{\varepsilon\varepsilon}=\frac{1}{\gamma}\text{Im}(Z_{\varepsilon\varepsilon})$, etc. are the dimensionless stiffness and damping coefficients, respectively.

III. Numerical Treatment of Steady-State and Dynamic Reynolds' Equations

In the present investigation, the stationary equation is solved using the Galerkin's finite element method while the dynamic equations are solved by means of the finite difference technique. Because of the axial symmetry of the bearing, so only the half bearing is divided into $N_\theta\times N_z$ equal rectangular cells (elements) with an area equal to $\Delta\theta\times\Delta\tilde{z}$ where $\Delta\theta=\frac{2\pi}{N_\theta}$ and $\Delta\tilde{z}=\frac{1/2}{N_z}$ are the mesh sizes in the circumferential and axial directions, respectively.

IV. Method of Solution

The steady-state solution of elastoaero dynamic problem which is considered as a highly nonlinear fluid-structure interaction problem is obtained by the substitution method. This method consists of building up a series of solutions $\{P_0^{(0)}\}$, $\{P_0^{(1)}\}$, ..., $\{P_0^{(k-1)}\}$, $\{P_0^{(k)}\}$; $\{P_0^{(k)}\}$being calculated from $\{P_0^{(k-1)}\}$by solving the linear system:

$$\left[K\left(P_0^{(k-1)}\right)\right]\left\{P_0^{(k)}\right\}=\left\{F\left(P_0^{(k-1)}\right)\right\};\ k=1,2,\ldots k_{max}$$

We can write this in incremental form by introducing the residual vector $\{R^{(k)}\}$:

$$\left\{R^{(k)}\right\}=\left\{R\left(P_0^{(k-1)}\right)\right\}=\left\{F\left(P_0^{(k-1)}\right)\right\}-\left[K\left(P_0^{(k-1)}\right)\right]\left\{P_0^{(k-1)}\right\}$$
$$\left[K\left(P_0^{(k-1)}\right)\right]\left\{\Delta P_0^{(k)}\right\}=\left\{R^{(k)}\right\}$$
$$\left\{P_0^{(k)}\right\}=\left\{P_0^{(k-1)}\right\}+\Omega_0\left\{\Delta P_0^{(k)}\right\}$$

where Ω_0 is a relaxation factor which ensures and accelerates the convergence of the iterative process.

To obtain the steady-state and dynamic solutions of elasto-aerodynamic problem, the following steps of the computational procedure are then performed:

1. Select the input parameters of the problem ε_0 , R, L, C , t_b , s , l , E , σ, ω, p_a, μ .
2. Initialize the iteration number k to *0*, the norm $\|n\|$ to *1.*, and the global vector containing nodal dimensionless steady-state pressures $\{P_0^{(k)}\}=1$.
3. While $(\|n\|>\varepsilon_p)$ and $(k<k_{\max})$, do

- Set $k \leftarrow k+1$
- Calculate the dimensionless steady-state film thickness profile using (4) for eachnode of the finite element grid
- Initialize global matrices [K] and {F} to 0.
- For each element:
  - Extract the elementary vector $\{p_0^{(k-1)}\}$ from the global vector $\{P_0^{(k-1)}\}$ as well as the elementary global coordinates arrays of each node by means of the connectivity array
  - Compute the elementary matrices $[k_e(p_0^{(k-1)})]$ and $\{f_e(p_0^{(k-1)})\}$ using the Gauss-Legendre quadrature
  - Assemble $[k_e]$in $[K]$, and $\{f_e\}$ in $\{F\}$
- Form the reduced matrices $[K_r]$ and $\{F_r\}$ by introducing the essential boundary conditions (9a) and (9b)
- Solve the reduced linear system $[K_r]\{P_{0_r}^{(k)}\}=\{F_r\}$for the reduced global pressure vector $\{P_{0_r}^{(k)}\}$using the successive over-relaxation (SOR) method to take into account the boundary condition (9c)
- Form the global pressure vector $\{P_0^{(k)}\}$from $\{P_{0_r}^{(k)}\}$and the values of boundary conditions
- Calculate $\{\Delta P_0^{(k)}\}=\{P_0^{(k)}\}-\{P_0^{(k-1)}\}$and the relative least square norm of $\{\Delta P_0^{(k)}\}$, i.e. $\|n\|=\dfrac{\sqrt{\langle\Delta P_0^{(k)}\rangle\{\Delta P_0^{(k)}\}}}{\sqrt{\langle P_0^{(k)}\rangle\{P_0^{(k)}\}}}$
- Update the global pressure vector: $\{P_0^{(k)}\}=\{P_0^{(k-1)}\}+\Omega_0\{\Delta P_0^{(k)}\}$

4. End do while
5. Calculate the steady-state lift force and the steady-state attitude angle ϕ_0
6. Code the nodes for which the steady-state pressure is greater than the ambient pressure. This step is necessary to solve the first order complex dynamic equations.
7. Solve the linear partial differential equations, (7) and (8) over the finite difference grid with SOR scheme to obtain the complex dynamic pressures $\widetilde{Q}_\varepsilon$ and $\widetilde{Q}_\phi$. It should be noted that the calculations are performed for each coded node belonging to the over-ambient region without vanishing the computed negative pressure terms. The pressure convergence criterion is $Max\left(\left|\dfrac{\widetilde{Q}_{\alpha_{ij}}^{(k+1)}-\widetilde{Q}_{\alpha_{ij}}^{(k)}}{\widetilde{Q}_{\alpha_{ij}}^{(k+1)}}\right|\right)\le 10^{-5}$ where the symbol $|\ |$ means here the magnitude of the complex quantity $\dfrac{\widetilde{Q}_{\alpha_{ij}}^{(k+1)}-\widetilde{Q}_{\alpha_{ij}}^{(k)}}{\widetilde{Q}_{\alpha_{ij}}^{(k+1)}}$, and $\alpha=(\varepsilon, \phi)$.
8. Compute the fluid-film complex impedances and deduce the stiffness and damping coefficients.

V. Results and Discussion

Based on the analysis described in the present paper, two separate computer codes were developed to study the effects of elastic deformations of the bump foil on the steady state and dynamic performance characteristics of a compliant air foil bearing using the algorithm described above.

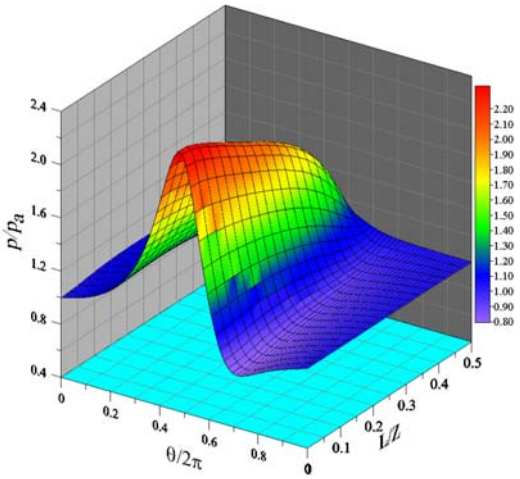

(a) Rigid gas bearing

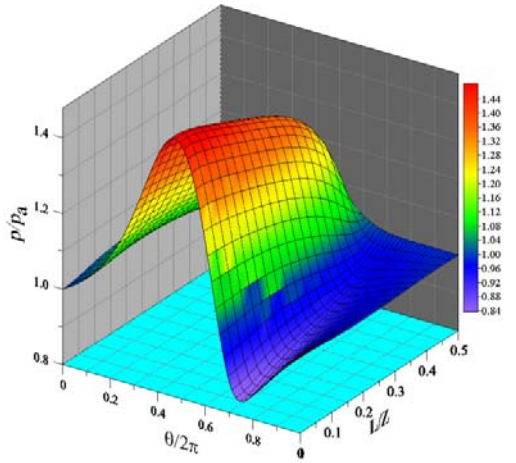

(b) Compliant gas foil bearing

Fig. 3 Steady-state pressure distributions

A. Effects of Elastic Deformations in Both Steady State and Dynamic Pressures

The calculations were performed for: $\Lambda = 1.07$, $\alpha = 0.4$, $R/L = 0.5$, $C/R = 2\times10^{-3}$ which are the steady-state eccentricity ratio, the compressibility number, the compliance factor, and the aspect and clearance ratios of the journal bearing, respectively. Fig. 3 depicts the steady-state pressure profiles and contours calculated in the half bearing for a highly loaded journal bearing operating at ε_0 =0.8. It is observed that the effect of the bump-foil elasticity leads to a spreading of the pressure distribution in the circumferential direction of the bearing over a greater area and to an important reduction of the peak pressure inducing a reduction of the journal bearing carrying capacity. The increasing of the fluid-film thickness over the whole bearing area explains the pressure drop.

It is also observed that the 3-D plots of the steady-state pressure field present sub-ambient pressures which occur in the divergent region of both rigid and compliant foil bearings. The existence of sub-ambient region provides the suction necessary to replenish the air pumped out by side.

In Figs. 4 and 5, we compare the distributions of real and imaginary parts of the complex dynamic pressure $\widetilde{Q}_\varepsilon$ calculated in the half bearing for rigid and compliant bearings and ε_0 =0.8. As found under steady-state conditions, the elastic deformations of the bump foil also affect the maximum value of both dynamic pressures and this effect is more pronounced when the dynamic deformation is considered in addition to the static one. Similar trends were observed for the real and imaginary parts of the dynamic pressure $\widetilde{Q}_\phi$.

Besides, it should be pointed out that almost similar trends were found for both rigid and compliant self-acting liquid-lubricated journal bearings (incompressible case) [10].

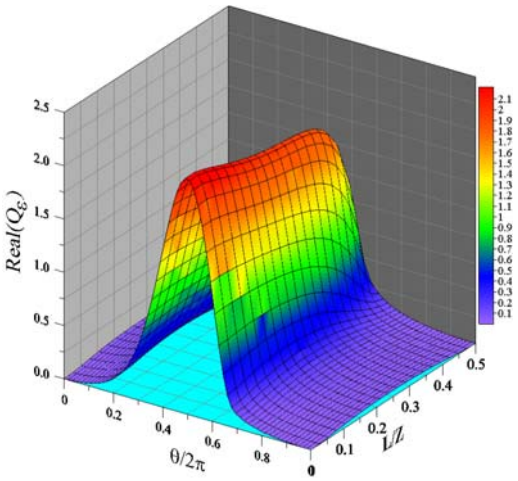

(b) α=0.4 (Static deformation only)

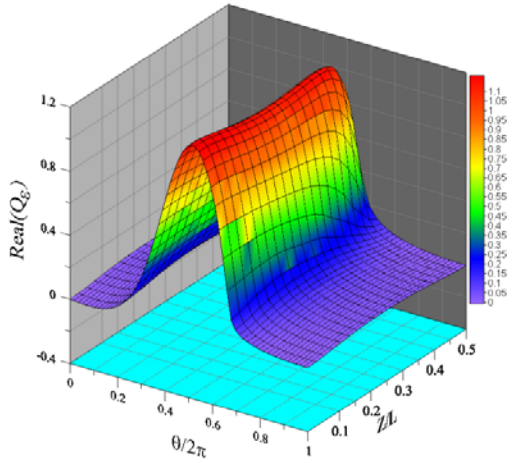

(c) α=0.4 (both static and dynamic deformations)

Fig. 4 Representations in 3D of the real part of the dynamic pressure $\widetilde{Q}_\varepsilon$

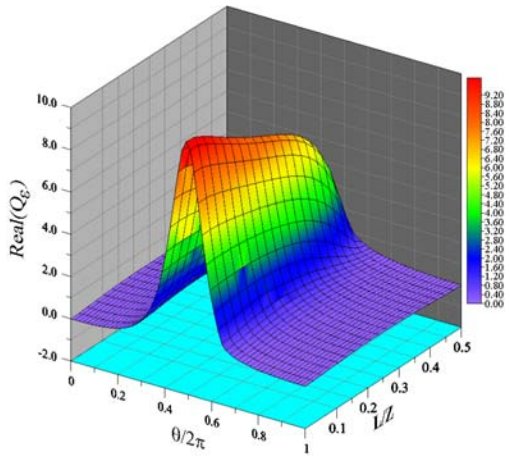

(a) α=0.0

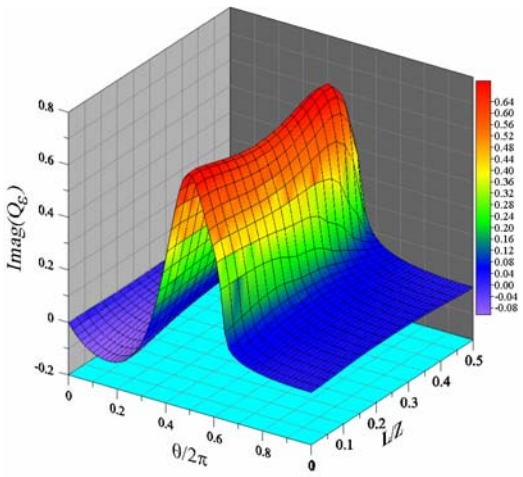

(a) α=0.0

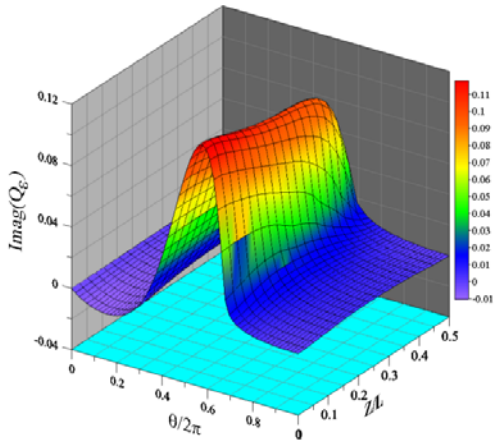

(b) α=0.4 (Static deformation only)

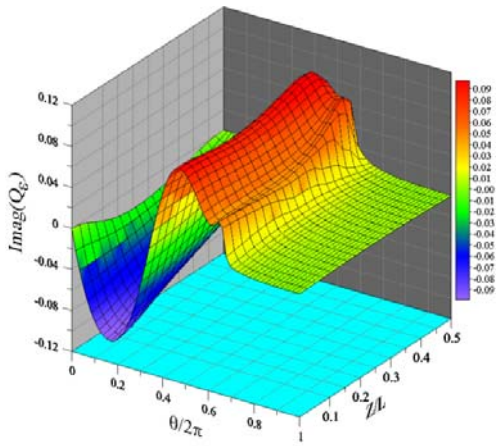

(c) α=0.4 (both static and dynamic deformations)

Fig. 5 Representations in 3D of the imaginary part of the dynamic pressure $\widetilde{Q}_\varepsilon$

B. Effects of Dynamic Deformations on the Dynamic Coefficients

In Fig. 6, stiffness and damping coefficients of the rigid air bearing are plotted as a function of excitation frequency ratio.

The rotor speed is*38krpm* and the steady-state eccentricity ratio is 0.8 (heavy load). The results show that the dynamic coefficients stay mainly constants for high values of the excitation frequency.

However, we observe a nonlinear evolution of these coefficients for lower frequency ratios. The direct stiffness coefficient in the load (vertical) direction a_{XX} is the largest and it increases as the excitation frequency ratio γ increases.

The direct stiffness coefficient in the horizontal direction a_{YY} displays similar behaviour, except that it peaks at a smaller value.

The cross-coupled stiffness coefficients a_{XY}, a_{YX}, and the direct stiffness a_{YY} are significantly smaller in magnitude than the direct stiffness in the vertical direction a_{XX} over the entire range of excitation frequency ratios investigated.

The damping coefficients decrease monotonically and converge with increasing excitation frequency ratio.

Furthermore, the values of cross-coupled damping coefficients b_{XY} and b_{YX} differ from each other significantly instead of being equal as predicted by the incompressible hydrodynamic lubrication theory.

It can be concluded that the excitation frequency sensitively affects the air foil bearing dynamic coefficients, and all the damping coefficients decrease in higher frequency region and vanish when $\gamma \to +\infty$.

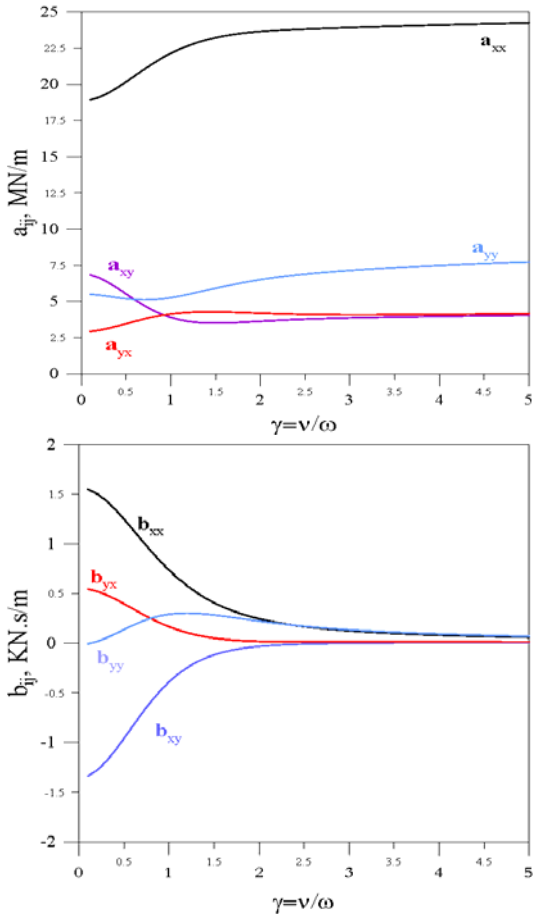

Fig. 6 Stiffness and damping coefficients of the rigid air bearing as functions of excitation frequency ratio

In Figs. 7 and 8, stiffness and damping coefficients calculated for a compliant foil bearing are plotted as a function of excitation frequency ratio for $\varepsilon_0 = 0.8$.

We observe that the elastic deformations of the bump foil significantly affect the eight dynamic coefficients over the entire range of excitation frequencies, and this effect is more pronounced when the dynamic deformation is considered in addition to the static one.

Compared to the rigid case, the taking into account of both static and dynamic deformations of the bump foil leads to an important reduction of stiffness and damping coefficients.

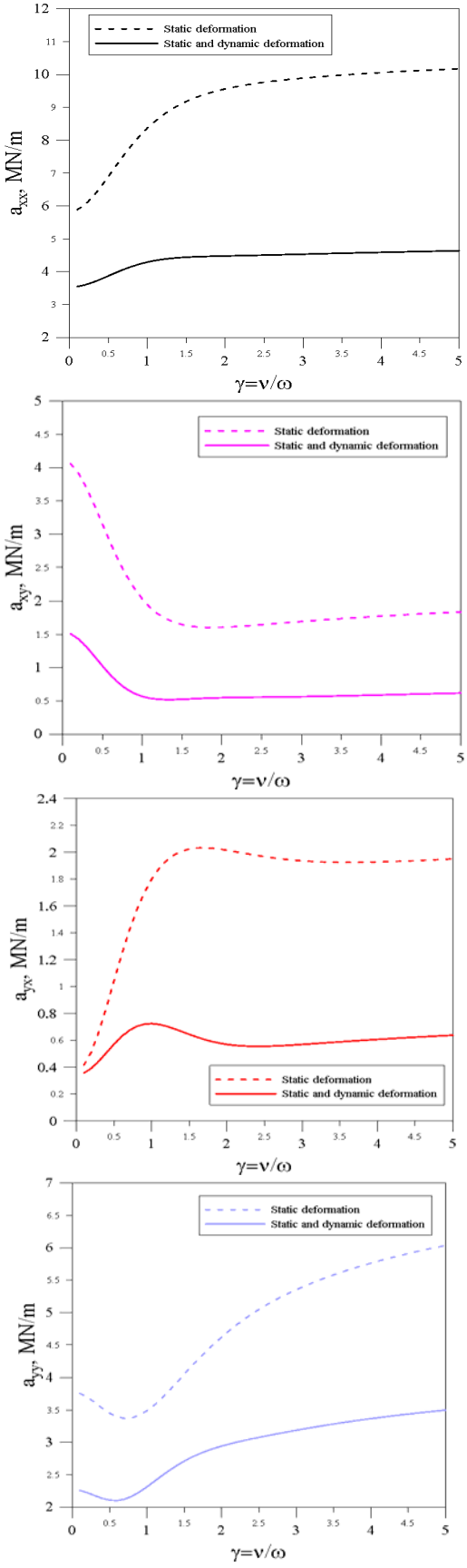

Fig. 7 Stiffness coefficients of the compliant air foil bearing as functions of excitation frequency ratio

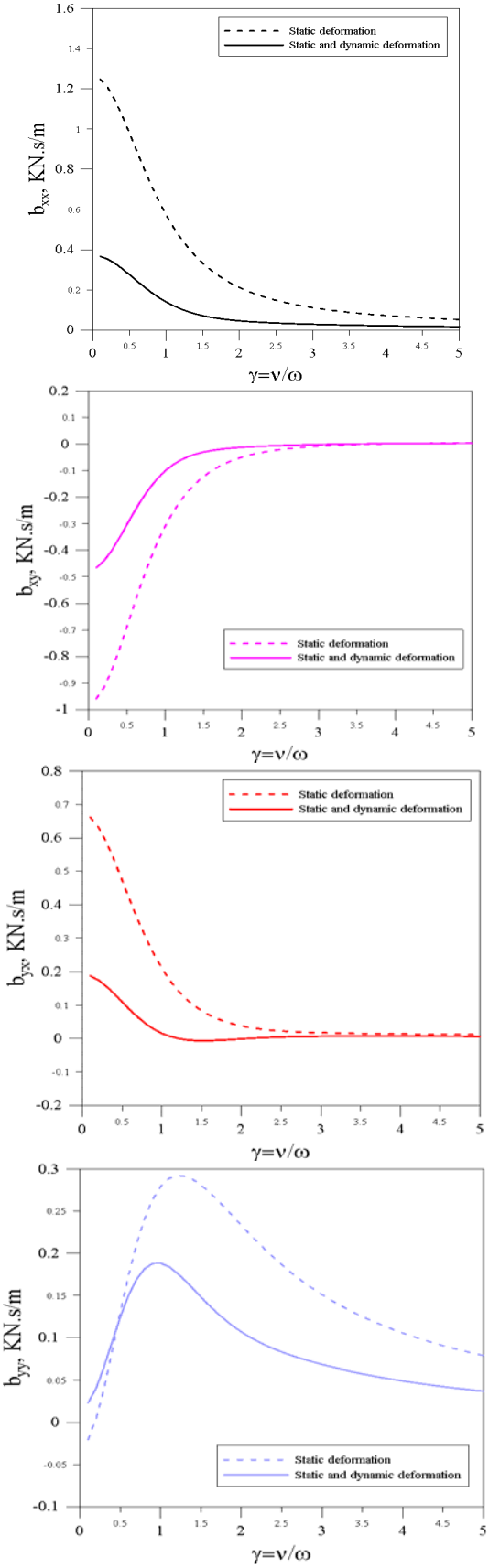

Fig. 8 Damping coefficients of the compliant air foil bearing as functions of excitation frequency ratio

VI. Conclusions

The following conclusions are drawn from the results obtained in this investigation:

1) The excitation frequency sensitively affects the air foil bearing dynamic coefficients even in the rigid case;
2) The elastic deformations of the bump foil affect the maximum value of both steady-state and dynamic pressures and this effect is more pronounced when the dynamic deformations are considered in addition to the static ones;
3) The taking into account of dynamic deformations of the bump foil leads to an important reduction of the stiffness and damping coefficients over the entire range of excitation frequencies.

References

[1] H.Heshmat, J. A.Walowit, O. Pinkus, "Analysis of gas-lubricated compliant foil journal bearings", *J. LubrTechn, Trans. ASME*, Vol. 105, pp. 647-655, 1983.
[2] J. P.Peng, M.Carpino,"Calculation of stiffness and damping coefficients for elastically supported gas foil bearings", *J.Trib. Trans. of the ASME,* Vol. 115, pp. 20-27, 1993.
[3] G.Grau, I.Iordanoff, B.Bou-Said, Y.Berthier, "An original definition of the profile of compliant foil journal gas bearings: Static and dynamic analysis",*J. Trib. Tran*., Vol. 47, no. 2, pp. 248-256,2004.
[4] Z. C. Peng, M.M.Khonsari, "A Thermohydrodynamic analysis of foil journal bearings", *J. Trib., Trans. ASME*, Vol. 128, pp. 534-541, 2006.
[5] M.Carpino, G.Talmage, "Prediction of rotor dynamic coefficients in gas lubricated foil journal bearings with corrugated sub-foils", *Trib. Tran.*, Vol. 49, no. 3, pp. 400-409, 2006.
[6] I.Iordanoff, B.Bou-Said, A.Mezianne, Y.Berthier,"Effect of internal friction in the dynamic behavior of aerodynamic foil bearings", *Tribo. Inter.*, 41, pp. 387-395,2008.
[7] L. S.Andrés, T. H.Kim, "Analysis of gas foil bearings integrating FE top foil models", *Trib. Inter.*, 42, pp. 111-120, 2009.
[8] Matta P., ArghirM., Bonneau O., "Experimental analysis of cylindrical air-bearing dynamic coefficients", *Trib. Tran*., 53, pp. 329-339, 2010.
[9] Paulsen B. T., Morosi S., Santos I. F.,"Static, dynamic, and thermal properties of compressible fluid film journal bearings", *Trib. Tran.*, Vol. 54, pp. 282-299, 2011.
[10] Lahmar M., Ellagoune S., Bou-Saïd B., "Elasto-hydrodynamic lubrication analysis of a compliant journal bearing considering static and dynamic deformations of the bearing-liner", *Trib. Tran*., Vol. 53,pp. 349-368, 2010.